HIGHLY TURBULENT HYDROGEN FLAMES

Nikolai Ardey
Lehrstuhl A für Thermodynamik
Technische Universität München
80290 Munich, Germany
+49 - 89 - 2105 3458

Franz Mayinger
Lehrstuhl A für Thermodynamik
Technische Universität München
80290 Munich, Germany
+49 - 89 - 2105 3436

Abstract

Within the scope of safety considerations for hydrogen processing plants as well as for nuclear reactors due to the considered release of hydrogen in the coarse of a severe accident considerable efforts are put on the investigation into the propagation of turbulent, premixed hydrogen-air - flames. The present paper gives a short review on the physics of turbulent reacting flows putting emphasis on the unstable dynamics of lean hydrogen-air flames and the interaction of flame fronts with vorticity of various scales. Turbulent flame acceleration is presented reporting on the experimental results of recent and former work on turbulent hydrogen deflagrations in cylindrical enclosures and the transition to detonation, which was performed at Lehrstuhl A für Thermodynamik. The diagnostics of turbulent reacting flows applied within the present work is based on sophisticated optical methods in order not to disturb the physical process itself by the sensor.

1. TURBULENT FLAME STRUCTURE BY HEAT AND MASS TRANSPORT

1.1. Development of Flame Turbulence and Instability of Lean Hydrogen Flames

The development of a turbulent flame front and its structure can not solely be deduced on the development of turbulent flow. From up the very beginning of the hemispherical growth of the flame kernel it interacts with its self generated pressure waves. The pressure waves propagating across the flame front with a pressure gradient ∇p, thereby, yield a considerable rotation when it superimposes the density gradient $\nabla\rho$ along the flame front due to baroclinic vorticity generation by $\nabla p \times \nabla\rho$ [1]. The flame front then starts to wrinkle and to form cusps towards the unburned mixture. This process works within acoustic time scales and is, therefore, decoupled from the interaction with flow vorticity.

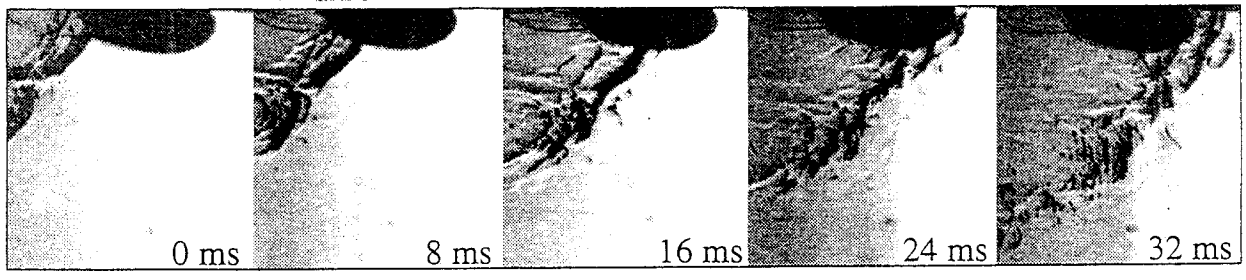

Fig. 1.1: Development of a cellular H_2-air-flame in a horizontal channel at 9 vol.% H_2, Schlieren-ciné-record of a flame front propagating in horizontal, 268×268 mm - flow channel. (The black spot at the top corresponds to a local obstruction of the 175×175 mm - observation window.)

The stability of the flame structure against these disturbances can be deduced from the stability of the boundary of a heavy fluid which is stratified upon a light fluid in a gravity field, which was investigated by Taylor [2]. Once a small cusp is formed towards the lighter fluid, it grows in the direction of gravity and entrains the lighter fluid in an unstable manner (Rayleigh-Taylor Instability). If the gravity is substituted by the pressure gradient, a similar situation is obtained for propagating flame fronts. Hence, the cusps grow into the unburned mixture by a Rayleigh-Taylor Instability and a cellular structure of the flame front is formed (s. fig. 1.1). The higher the pressure gradient across the flame front the finer the cellular structure is to be observed (s. fig. 1.2).

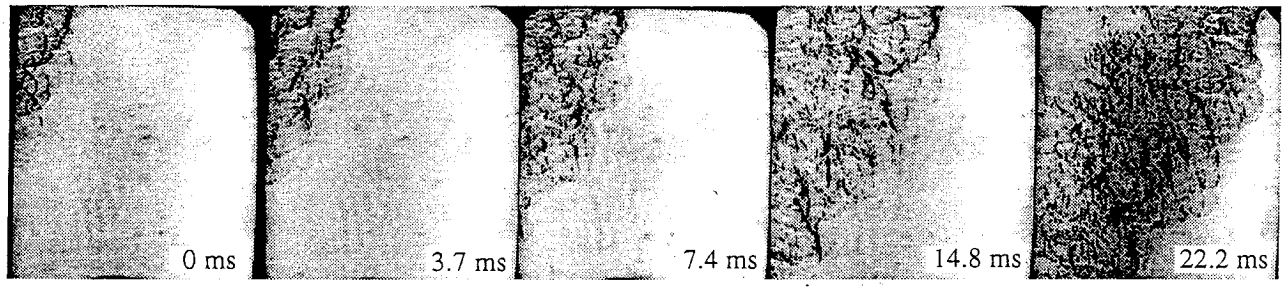

Fig. 1.2: Schlieren record of a propagating H_2-air-flame front at 12 vol.% H_2 with a fine scale - cell structure

Especially for lean hydrogen flames the unstable formation of cusps towards the unburned mixture is strongly enhanced by molecular transport phenomena right ahead of the flame. Surface enlargement due to positive curvature enhancement by cusp formation leads to larger preheating zones with increasing heat losses of the reaction zone by thermal diffusion. As a stabilizing effect the molecular heat transport competes with material diffusion of the deficient reactant (H_2 in the lean case). Enlarged preheating zones at positive curved cusps contain more molecules of this reactant to be transported into the reaction zone by mass diffusion. The corresponding negative curved flame sections with a diminished preheating zone contain accordingly less molecules of the deficient reactant. I.e. the effective laminar burning velocity appears to be higher at the crest of the cusp and lower at the corresponding trough in comparison to the average laminar burning velocity of the mixture. Due to the high diffusivity of H_2 in air the latter mechanism dominates the stabilizing thermal effect and, thereby, introduces additional instability for the cusp formation. The dominating effect of H_2 diffusion against thermal diffusion expresses itself by a low *Le* number (about 0.3 - 0.5), which is the ratio between the mass diffusivity D_{H2} and the thermal diffusivity $a=\lambda/(\rho c_p)$:

$$Le = a/D_{H2} \qquad (1)$$

Fig. 1.3 shows the cross-section of upward propagating H_2-air flame fronts superimposed by a steady flow in a vertical, rectangular flow channel of 60×26 mm. The flame fronts were visualized by OH-fluorescence, excited by a thin, ultrashort-pulsed laser lightsheet at 308 nm (Laser Induced Fluorescence, LIF) and detected by a UV-intensified CCD-camera [3]. Due to the preferential diffusion of H_2 the reaction rates obviously reach a minimum at the negatively curved sections, which results in partial quenching and interruptions of the flame front at these locations, whereas the reactivity reaches a maximum at the crest of the cusps.

1.2. Flame Vortex Interaction and Flame Stretching

Due to the unstable dynamics of a cellular H_2-air-flame the structure of the flame is subjected to a continuous change and reformation of cells yielding a complex, highly turbulent

flow field right ahead of the flame, which gets into interaction with the flame front itself on a longer time scale as the acoustic interactions. The turbulent flow field comprises of a vortex cascade starting with eddies of integral length scale L, which dissolve in smaller eddies (e.g. of Taylor micro scale λ_T) and ending up with the smallest correlated fluid motion (Kolmogorov micro scale k) before the rotational energy dissipates to uncorrelated thermal motion. Whereas macroscopic eddies of integral length scale wrinkle the flame surface by macroscopic flame stretch and curvature enhancement, small scale vorticity entrains the reaction zone and enhances fine scale mixing. The effect of the flame vortex interaction on the effective, turbulent burning velocity s_t depends on the competition between incitement by surface enlargement or enhanced turbulent transport and turbulent quenching with high fluctuating velocities u' separating reacting species or by thermal quenching with a high flame stretch that can not be compensated by molecular transport. A comparison of the life times of the different eddies with the chemical reaction time leads to a subdivision into different combustion modes, which were summarized in a phase diagram by Borghi [4] and Peters [5], that appeared to be a valuable tool for the general assessment of combustion processes in any turbulence regime. A comprehensive discussion of the different combustion modes is to be found in [5].

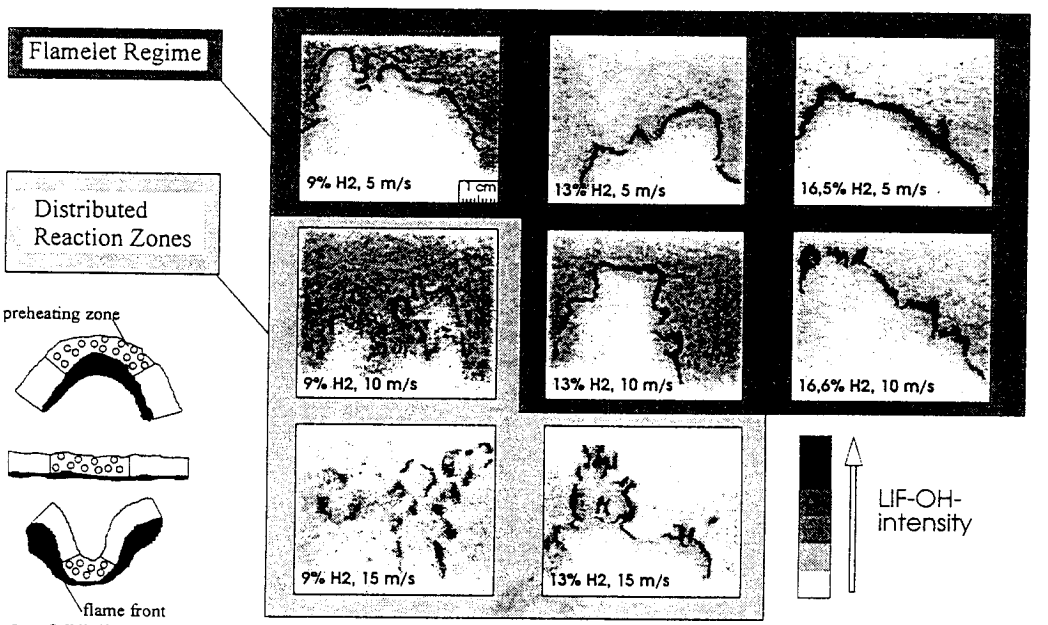

Fig. 1.3: OH-LIF-images of upward propagating flame fronts superimposed by a steady flow in a vertical, 60×26 mm flow channel.

Turbulent quenching generally arises, when the lifetime of the smallest eddies (Kolmogorov micro eddies) dissolve earlier than the chemical reaction of the involved molecules is finished, i.e. the ratio of the chemical reaction time τ_c and the lifetime of the Kolmogorov eddies τ_k (Karlovitz number $Ka=\tau_c/\tau_k$) is higher than unity. Below that limit the flame fronts are generally envisaged as thin, continuous and locally laminar reaction zones completely separating burnt and unburned gases to be properly described by fast chemistry approaches (flamelet regime) (s. fig. 1.3). Incitement of the turbulent burning velocity is achieved in this regime mainly by surface and curvature enlargement. Beyond the limit of $Ka=1$ flame stretch causes partial quenching and reaction zones are thickened due to the entrainment of Kolmogorov-small

scale vorticity yielding maximum strain rates (distributed reaction zones) (s. fig. 1.3). Abdel Gayed et al. found a quenching criterion within the regime of distributed reaction zones, given by the product of the Karlovitz flame stretch factor K and the Lewis number Le:

$$(K\,Le)_q = 1.5 \;;\; K = \frac{u'}{s_l}\frac{\delta_l}{\lambda_T} \qquad (2),$$

stating that flame surface enlargement predominates the reduction of local chemical reaction rates by turbulent quenching below that limit and the other way around. Hence, flame speeds reach a maximum value at the limit of $(K\ Le)_q = 1.5$ [6]. Taking into account the correlations between the different turbulent length scales by the viscous energy dissipation rate ε, which are to be found e.g. in [7], the quenching criterion can be applied to the integral length scale L, which is easier accessible by flow diagnostics and depends on the geometrical flow situation:

$$K = 0.157\left(\frac{u'}{s_l}\right)^2 \mathrm{Re}_L^{-0.5} \quad ; \quad \mathrm{Re}_L = \frac{u'L}{\nu} \qquad (3)$$

1.3 Modeling of Turbulent Burning Rates

Based on experimental data on the turbulent burning rates huge efforts were put on the modeling of the turbulent burning rate as a function of flow- and mixture parameters. As a very first approach the incitement of the turbulent burning rate was modeled as a linear function of the turbulent fluctuating velocity $s_t/s_l = 1 + u'/s_l$ ignoring turbulent quenching phenomena [8]. Others describe the turbulent burning rate as a function of the flame surface enlargement, which again is a function of u', L, and mixture properties [9], [10]. Since the integral turbulent burning rate does not only depend on the flame surface but also on the flame thickness and the curvature distribution and the flame structure changes strongly when turbulent quenching gets involved, a more general description is necessary. Reasonable agreement of experimental and calculated data could be achieved with models describing the incitement of the turbulent burning rate as a function of $(Re_L)^{0.5}$ [11] or at least $(u')^{0.5}$ and the turbulent quenching as a function of $-(u')^2$. Andrews et al. give a comprehensive survey on proposed model approaches [7]. A recently improved model for the turbulent burning rate has been derived by Beauvais [12], which is based on experimental data from explosion tube experiments with H_2-air mixtures in a horizontal 6m - tube with a diameter of 66 mm. The turbulent burning rate was taken from the difference of the flow velocities right ahead of the flame and just behind it and a momentum and energy balance (see fig. 1.4). The transient flow velocity and the corresponding fluctuations during flame propagation was measured by means of a two component Laser-Doppler-Velocimeter (LDV) at an optical accessible section of the tube. Applying an obstacle path of various blockage ratios and obstacle spacings the turbulence intensity was varied.

Taking into account the turbulent quenching limit from Abdel Gayed et al. (2), (3) and assuming a Prandtl number of 1 Beauvais derived the following burning law for the turbulent burning velocity, which reasonably fits the experimental data (see fig. 1.5) [12].

$$\left(\frac{s_t}{s_l}\right) = 1 + b\sqrt{\frac{L}{\delta_l}}\left(\sqrt{\frac{u'}{s_l}+1}-1\right) - c\left(\frac{u'}{s_l}\right)^2 \quad ; \quad c = \frac{0.157\,b\,Le}{4\,(KLe)_q} \qquad (4)$$

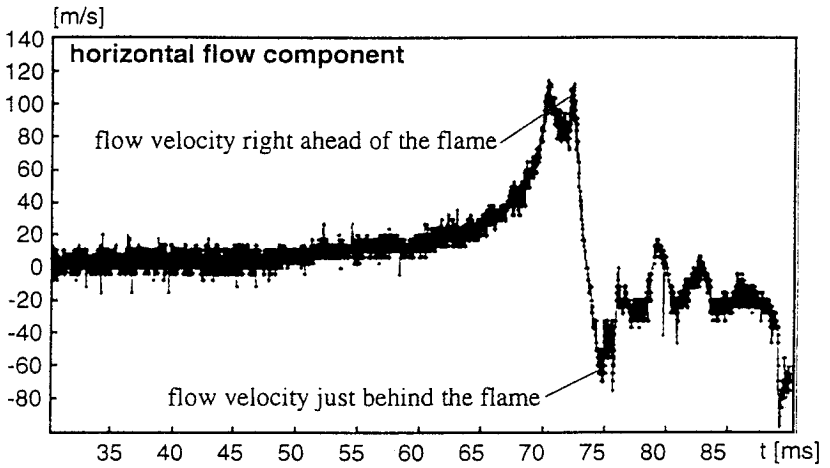

Fig. 1.4: LDV-record of the horizontal flow component during flame propagation [12].

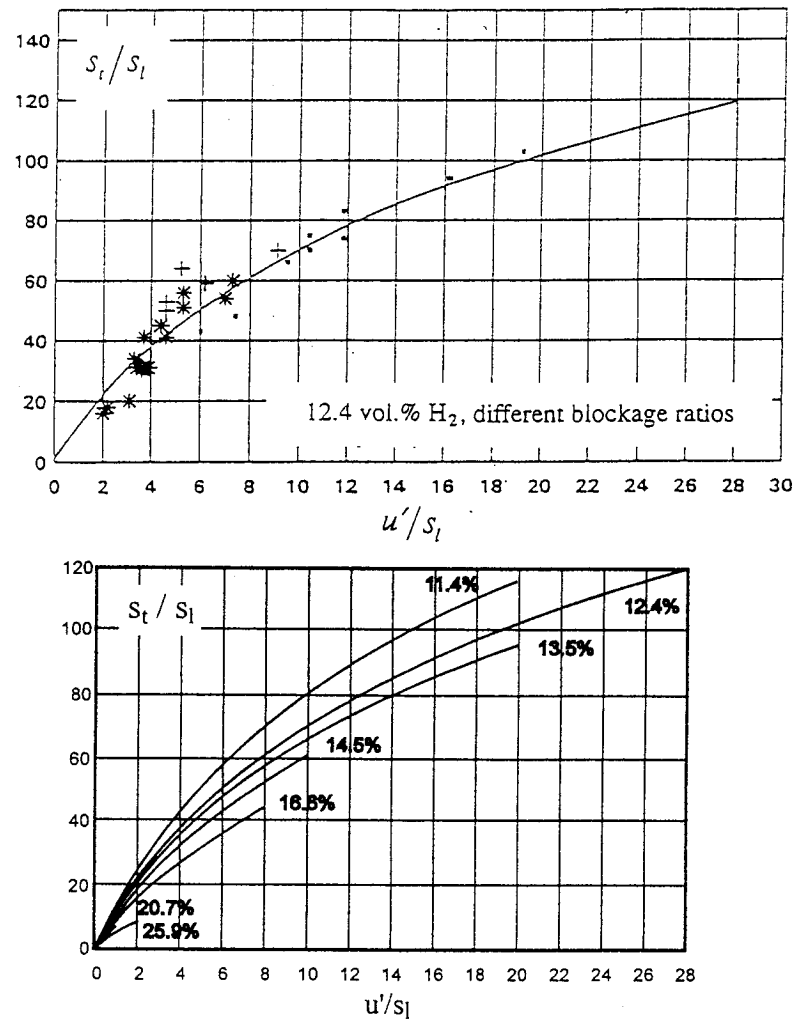

Fig. 1.5: Top: Turbulent burning rates as a function of u', comparison of model (4) and experimental data; bottom: parametric curves for the turbulent burning rate at various H_2-concentrations.

The parametric curves for the turbulent burning rate in fig. 1.5 show obviously an increasing sensibility for turbulent incitement of the flame with decreasing H_2-concentrations. This behavior is a contradiction to the stronger effect on flame stretch by a certain vorticity for lean flames than for rich ones due to an increasing flame stretching factor K (2) with decreasing H_2-concentrations. One reason for that behavior is the decreasing resistance, which the flame

front offers to the distortion by a vortex with decreasing H_2-concentrations with respect to a decreasing pressure gradient across the flame front. A second effect is caused by an increasing instability through preferential diffusion with decreasing H_2-concentrations due to a decreasing *Le* number with leaner flames and an increasing importance of the diffusive instabilities with leaner flames (since the deficient reactant is the more deficient the leaner the concentration). It is proved by various experiments at elevated initial temperatures in a range of ambient to 280°C that the remaining constant *b* in (4) is not dependent on the initial temperature, i.e. the temperature effect is captured by the model itself. However, the constant b varies still with the equivalence ratio (from 2.62 for 13.5 vol.% H_2 to 3.98 for 11.4 vol.% H_2) pointing at the effect of diffusive instabilities, which is disregarded by the theory the burning law of (4) bases on. Although this effect is commonly understood, there is no burning law available, for the time being, that considers the *Le*-number effects in a closed manner, which is still an open task for further model improvement.

2. TURBULENT FLAME ACCELERATION

2.1 Interaction of Flame Fronts with Low Blocking, Single Obstacles

Hydrogen explosions in confined enclosures can be considered as a superimposition of the turbulent burning behavior according to eq. (4) and a highly turbulent expansion flow generated by the combustion induced heat release and acoustic effects due to the interaction with sent out and reflected pressure waves. The dynamic pressure loads on the confining walls are strongly dependent on the propagation speed of the explosion. Immediately after the ignition of a H_2-air mixture at the end of an explosion tube an unstable feed back mechanism arises, when the cellular flame structure develops (ref. sect. 1.1) and generates turbulence ahead of the flame, which gets into interaction with the flame front yielding turbulent flame acceleration. Since the turbulence intensity in a smooth channel normally does not exceed a value of about 9%, the accelerated flame front turns into a steady propagating flame front with a constant velocity below the mixture limit for critical flame speeds with strong precursor shocks. Further flame acceleration can only be achieved by additional turbulence generation in the expansion flow ahead of the flame e.g. by flow obstacles.

In order to improve the understanding of the influence of flow obstacles on the flame propagation, experiments are presently performed in a horizontal, square cross section explosion tube (268×268 mm) with a length of 3.5 m. Single flow obstacles with representative geometries for typical equipment of technical facilities like tubes, grids, and other half size bodies are exposed to the propagating flame front at the middle of the tube (see fig. 2.1). The blockage ratio of each obstacle is below 15%.

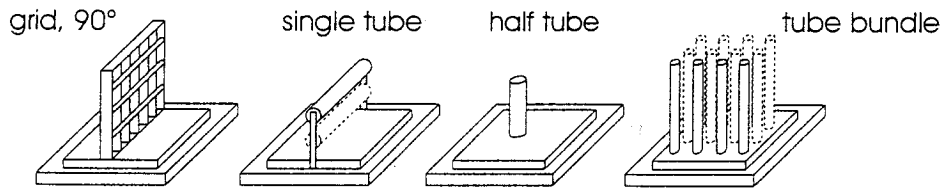

Fig. 2.1: Applied obstacles for the investigation into flame-obstacle interaction phenomena

Fig. 2.2 shows a representative selection of high-speed Schlieren ciné records of the flame propagation in the vicinity of a vertical half tube and a horizontal tube at different locations. When the more or less smooth flame front of a 9 vol.% H_2-flame creeping along the top wall of the tube passes the vertical half tube, a turbulent wake flow region behind the obstacle can be observed due to the irregular structure of the Schlieren record, which dissolves as soon as the wake flow region is burned out and the obstacle submerges completely in the burned

gas region. At the top of the obstacle the cellular structure bellies slightly due to the volume displacement by the obstacle. Since only a comparatively small part of the flame front is affected by the obstacle, there is not any remaining effect of the obstacle to be observed after a certain distance behind the obstacle. The increasing turbulence of the flame front with increasing H_2-concentrations prevents early flow separation at the tube and the volume of the wake flow zone decreases, which can be observed from the 12 vol.% H_2-flame in the vicinity of the vertical half tube. The wake flow zone does not cover the total height of the obstacle. With respect to the larger flame surface at 12 vol.% H_2, which covers the whole cross section of the tube, the affected part of the flame front by the obstacle is even smaller in comparison with the 9 vol.% H_2-flame. Measurements of the integral flame propagation speed in the explosion tube by means of equally spaced thermocouples and photo diodes with the vertical half tube do not exhibit any difference to the experiments without any obstacle.

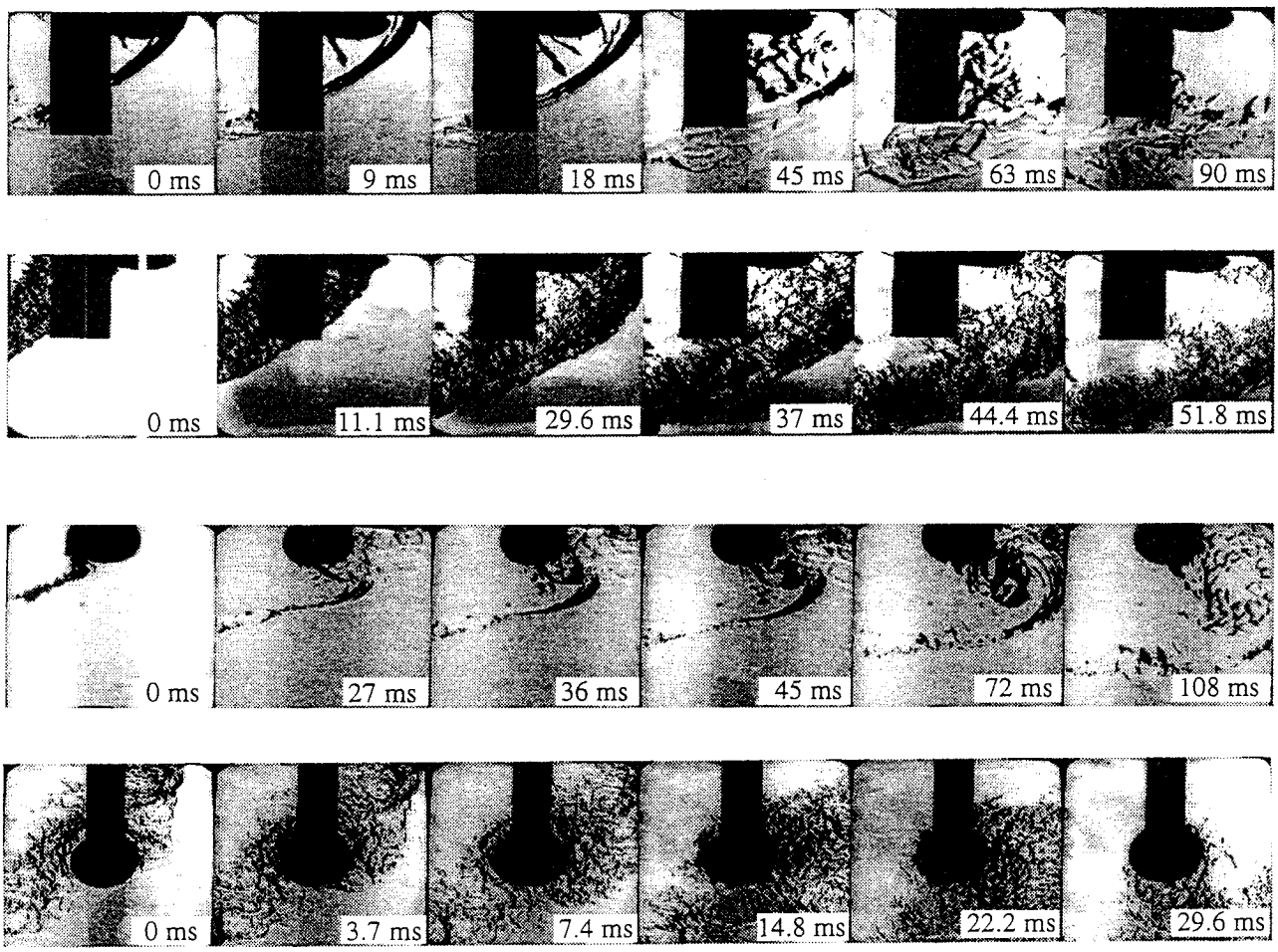

Fig. 2.2: High speed Schlieren ciné records of flame fronts propagating in the vicinity of flow obstacles, top: 9/12 vol.% H_2, vertical half tube; bottom: 9/12 vol.% H_2, horizontal tube.

This situation changes slightly, when the flame front interacts with the horizontal tube along the tube-obstacle axis, which covers the whole cross section of the explosion tube. Since the 9 vol.% H_2-flame just creeps along the top wall of the tube and covers mainly the upper half part of the tube, the obstacle was exposed to the flame front in the center of the upper half part of the tube, which corresponds to the upper border of the observation window. Hence, only the part below the obstacle axis is visible. The part between the obstacle an the top wall of the explosion

tube represents a smoothly narrowing channel causing a slight flame acceleration due to the slightly accelerated flow, which fades away just behind the obstacle. The flame part passing the lower boundary of the obstacle freely evades the obstacle due to the volume displacement. The accelerated flame part above the obstacle submits pressure waves, which are stronger than the pressure gradient across the flame front below the obstacle. These pressure waves push the flame front back at the lower boundary of the obstacle, whereas the flame parts away from the obstacle burn more or less unobstructed. The flame front consequently starts to roll up and to form a large scale vortex cylinder. It is of particular interest that the large scale flame vortex cylinder stagnates behind the obstacle. Apparently it is continuously fed by unburned gases, which are rolled in along the outer surface of the vortex. In spite of these obvious phenomena the integral flame speed along the axis of the explosion tube is just hardly affected. Thermocouple measurements along the top wall of the tube show a slightly accelerated motion of the flame front which reaches about twice the velocity than the velocity at the beginning of the tube (s. fig. 2.3), i.e. the upper part of the flame is some how decoupled from the stagnating vortex.

For the 12 vol.% H_2-flame the horizontal cylinder was located right in the center of the tube, since the 12 vol.% H_2-flame covers the whole cross section of the explosion tube representing a more or less symmetrical problem. Due to the highly turbulent properties of the flame front there is not any flow separation at the obstacle surface to be observed. Nevertheless the highly turbulent cellular parts of the flame obviously grow behind the obstacle causing a slight flame acceleration again up to about twice the velocity than the velocity at the beginning of the tube, which could be observed throughout the whole regime of H_2-concentrations investigated (s. fig. 2.3).

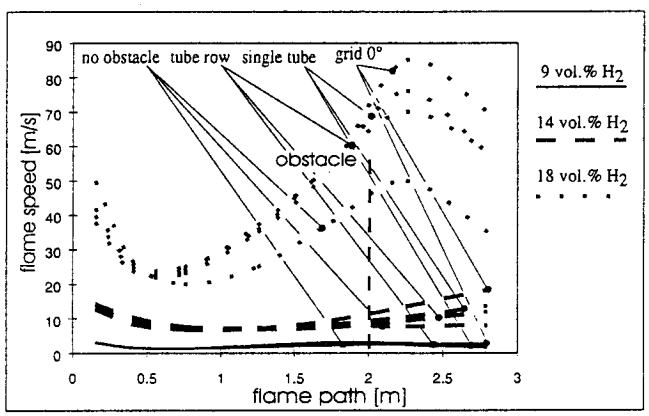

Fig. 2.3: Flame propagation speeds along the tube axis for different obstacles at 9, 14 and 18 vol.% H_2

2.2 Turbulence Promotion by Periodically Appearing, Low Blocking Obstacles

It can be concluded from section 2.1 that single obstacles with a low blockage ratio do not enduringly accelerate propagating flame fronts. The effects of flame obstacle interaction remain limited almost to the obstacle vicinity. Generally the turbulence intensities behind such a single obstacle do not reach the limits for strong turbulent quenching, i.e. the local flame acceleration is dominated by surface and curvature enlargement rather than by fine scale mixing and turbulent quenching. However, if multiple repeated obstacles are exposed to the propagating flame front this process can build up to a strong flame acceleration. Fig. 2.4 shows flame propagation speeds along the Ø66mm/6m-explosion tube with an obstacle path of repeated, 30%-blocking orifices [13]. Even at H_2-concentrations below 12 vol.% a considerable flame acceleration is achieved within the obstacle path which is the result of an unstable feed back mechanism between the flame front and the expansion flow ahead of the flame. When the flame front is slightly

accelerated after the first obstacle, the turbulent fluctuations increase due to the interaction of the accordingly accelerated expansion flow with the next obstacle. This again accelerates the flame front with respect to the turbulent burning law (4) generating even higher turbulent fluctuating velocities at the next obstacle e.t.c.. A schematic view of this feed back mechanism is displayed in fig. 2.5.

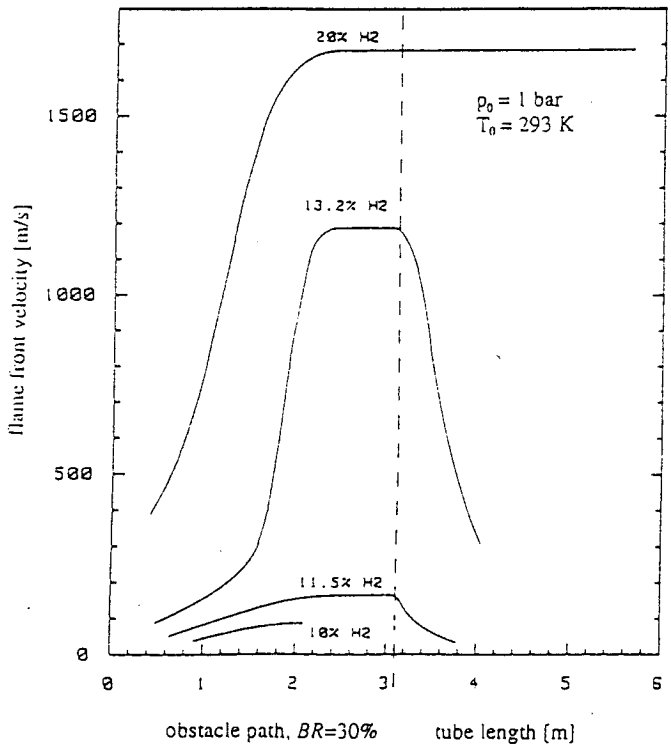

Fig. 2.4: Flame propagation speeds along the axis of a ∅66mm/6m-explosion tube with an obstacle path of repeated, 30%-blocking orifices with different H_2-concentrations [13].

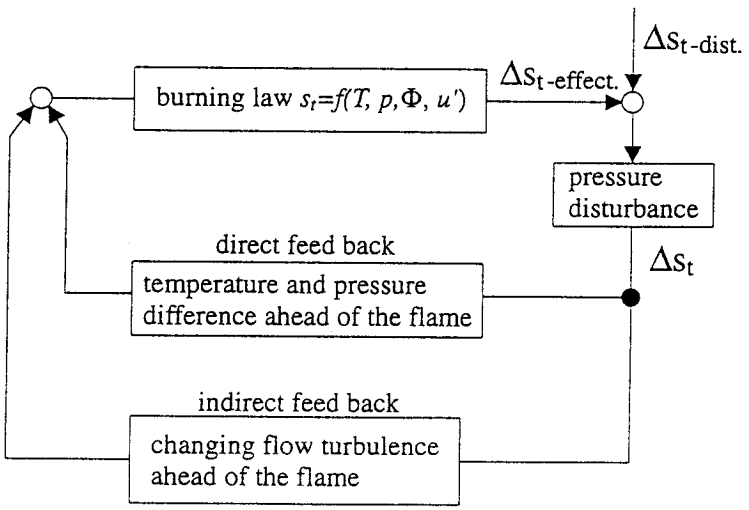

Fig. 2.5: Unstable feed back loop for flame acceleration within a field of repeated obstacles [13].

A significant transition to critical flame speeds is to be observed at H_2-concentrations above 12 vol.%. The sudden increase of the flame acceleration at 13.2 vol.% H_2 corresponds to the generation of a strong precursor shock wave by a sufficiently strong energy release of the reaction front. The precursor shock wave pre-compresses and pre-heats the unburned mixture in front of the reaction front, which, thereby, is accelerated. Further acceleration of the reaction front is achieved by an enlarged, highly turbulent boundary layer and complex shock reflections

within the obstacle field behind the precursor shock wave. The shock wave, at its part, is amplified by the accelerated reaction front. Again an unstable feed back mechanism of flame acceleration arises which leads to a decreasing distance between shock wave and reaction front and, hence, to an increasing coupling of reaction front and precursor shock. The unstable flame acceleration by shock flame interaction is generally limited by heat- and momentum losses near the confining wall of the tube (thermal choking). If the heat- and momentum losses are not high enough to avoid a shock wave amplification by coherent energy release in the reaction front (SWACER-mechanism, [14]), the reaction front gets into a direct coupling with the precursor shock and ends up in a self sustainable detonation, which remains stable even within the smooth section of the tube (s. fig. 2.4 at 20 vol.% H_2). Other wise the flame front remains at critical conditions within the obstacle path without a transition to a detonation and decays within the smooth section of the tube (s. fig. 2.4 at 13.2 vol.% H_2).

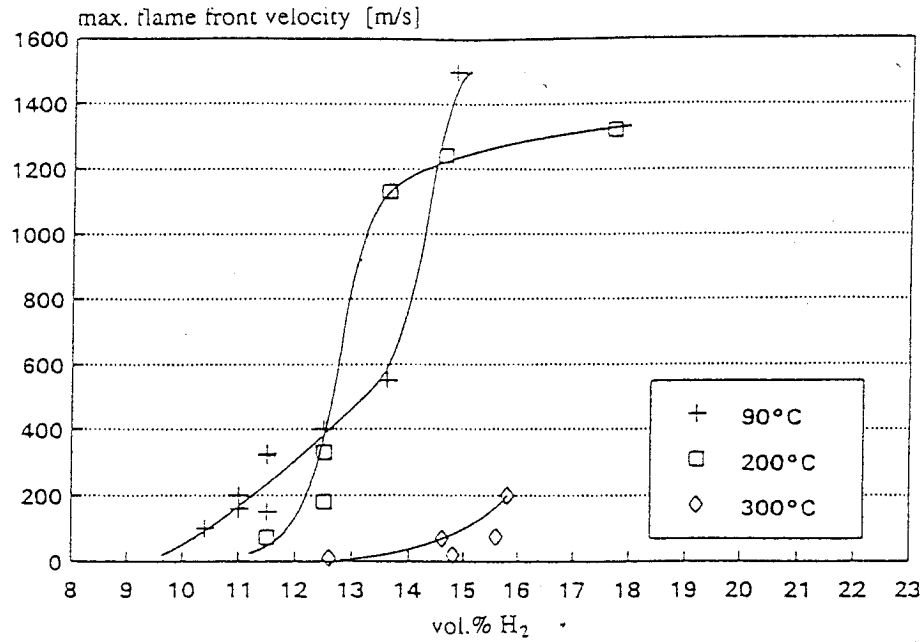

Fig. 2.5: Maximum flame speeds in a Ø66mm/6m-explosion tube with elevated initial temperatures and a 30% blocking obstacle path [12]

The importance of the unstable feed back of the turbulent expansion flow and the flame front can be derived also from the experiments at the Ø66mm/6m-explosion tube with elevated initial temperatures. First of all, the turbulent burning rate increases with increasing initial temperatures due to an increasing laminar burning velocity (ref. eq. (4)). Hence, the limits for the transition to critical flame speeds drop down to lower H_2-concentrations with elevated initial temperatures, which can be observed e.g. for an initial temperature of 200°C in comparison to an initial temperature of 90°C (s. fig. 2.5). But surprisingly the maximum flame speeds at 200 °C are less than the maximum flame speeds at 90°C below 12 vol.% H_2 and for the mixture with an initial temperature of 300°C a transition to critical flame speeds even does not occur within the whole range of H_2-concentrations investigated. This effect can be explained by a decreasing expansion ratio across the flame front at increasing initial Temperatures yielding a weaker expansion flow. That is, the turbulent fluctuating velocities ahead of the flame are accordingly weakened and the feed back mechanism for turbulent flame acceleration in a field of repeated obstacles is slowing down. Therefore, a flame front in a preheated mixture requires a longer run up distance in an obstacle field of a certain blockage ratio for the transition to critical flame speeds than a flame front in a cold mixture, although the transition occurs at lower H_2-concentrations with elevated initial temperatures, if the obstacle path is long enough.

2.3 Interaction of Flame Fronts with Highly Blocking Obstacles

Obstacles with a blockage ratio above 50% cause a strong flow contraction at the obstacle aperture. Behind the obstacle a flow jet separates, which is surrounded by a highly turbulent shear layer with turbulence intensities that are high enough to cause partially strong turbulent quenching. However, partial turbulent quenching is closely linked to strong flame acceleration, even by one single obstacle. To demonstrate this effect, OH-LIF-images were taken of flame fronts passing a baffle with a blockage ratio of about 60% in a vertical, rectangular flow channel of 60×26 mm (s. fig 2.6). A steady flow of 5 to 15 m/s was superimposed to the flame propagation in order to vary the turbulent fluctuation velocity u'. Phylaktou et al. [15] specified the obstacle induced turbulence intensities in the shedded shear layer behind baffles of BR=60% to reach values of about 0.6. The obtained flow strain rates are just below the quenching criterion of $(K\ Le)$=1.5 with a steady flow of 5 m/s and reach the limit with 10 m/s respective exceed the limit at 15 m/s. The corresponding strong quenching effects clearly turn out in fig. 2.6.

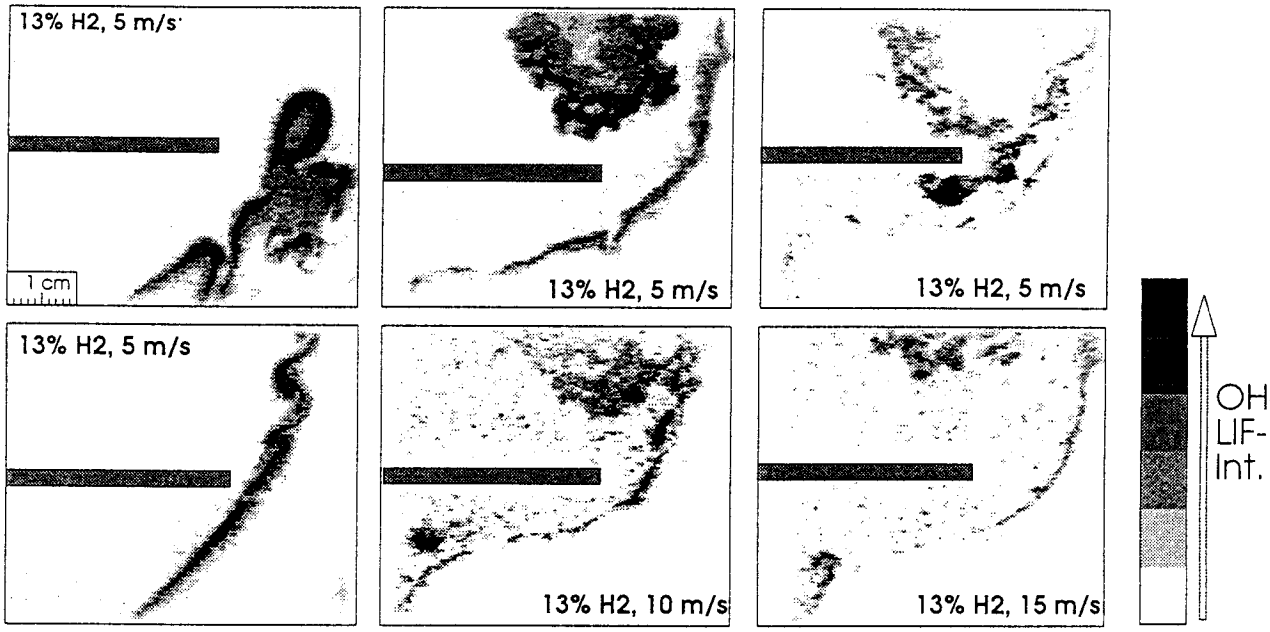

Fig. 2.6: OH-LIF images of H_2-air flames passing a baffle with BR=60% in a vertical flow channel of 60×26 mm with a superimposed steady flow of 5 - 15 m/s

Although only single shot images were obtained for the flame fronts passing the obstacle, the development of the flame structure could be reconstructed evaluating quite a number of single shots representing different time steps of the event. Following the flow contraction in front of the obstacle the flame front appears intensely corrugated in comparison to the undisturbed flame shape. When the flame front entrains the wake-flow zone, it is superimposed by the vortices separating at the edge of the obstacle.

Unburned radicals originating from aborted chemical reactions from the turbulent quenching zones are "washed out" from the shredded reaction zones and transported ahead of the flame by the accelerated jet flow showing high velocity-components tangential to the leading flame contour. Hence, the flame propagation is strongly disturbed right in the vicinity of the obstacle. When the partially quenched flame front reforms at a certain distance behind the

obstacle, where the turbulent flow strain is decayed, it becomes much more wrinkled and convoluted than it was before the obstacle due to the distribution of the small reacting shreds. Running into the region, which is enriched by unburned radicals originating from highly turbulent quenching zones, the flame becomes strongly accelerated. In sensitive mixtures for the transition to critical flame speeds local explosions are likely to occur in the radical-enriched zones, which can amplify themselves to detonation waves. The latter mechanism is generally referred to as "hot jet ignition". That is, turbulent quenching is closely linked to severe flame acceleration and the transition do detonation as a triggering mechanism. Recently performed experiments in a square cross section explosion tube (268×268 mm) with a length of 3.5 m applying a single obstacle with a 85% blocking, rectangular aperture confirm the strong flame accelerating effect of highly blocking obstacles (s. fig. 2.7). The flame propagation speeds were detected by a set of fast responding, UV-sensible photo diodes.

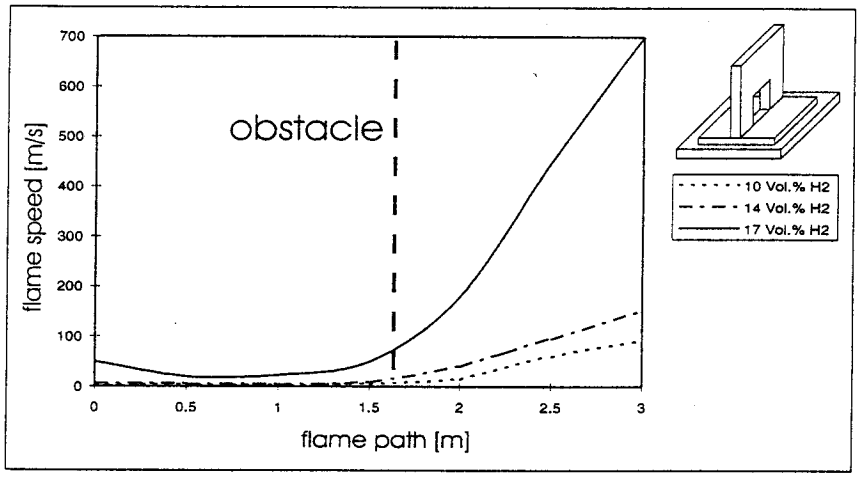

Fig. 2.7: Flame propagation speeds along the axis of a square cross section explosion tube (0.268×0.268×3.5) with a single obstacle with a 85% blocking, rectangular aperture.

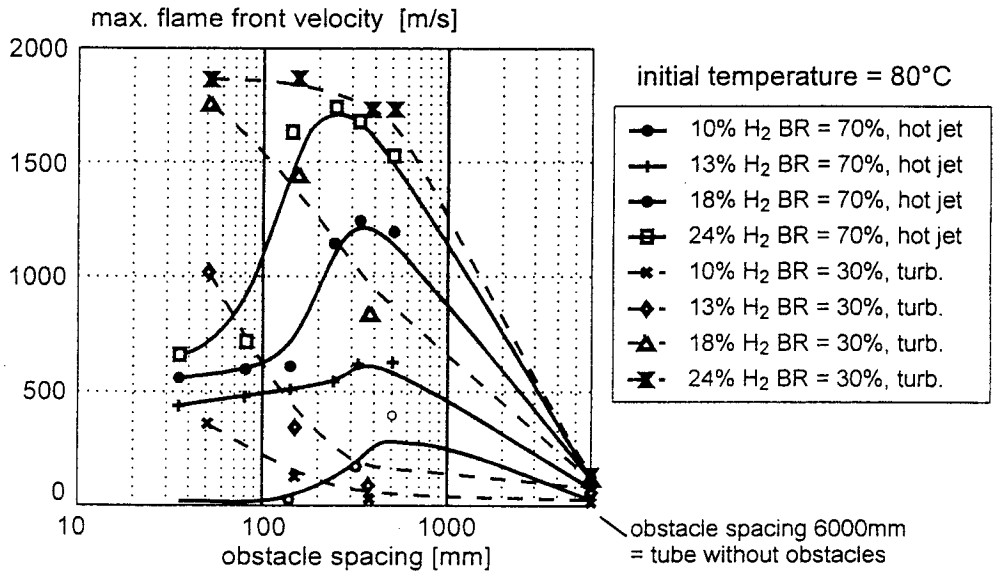

Fig 2.8: Maximum flame speeds in an obstacle path of different blockage ratios depending on the obstacle spacing [12]

Applying multiple repeated obstacles of a high blockage ratio leads to the same feed back mechanism for a strong flame acceleration like in the field of repeated, low blocking obstacles (ref. sect. 2.2), as it turned out from experiments in the Ø66mm/6m-explosion tube with an obstacle path consisting of 70% blocking orifices [12]. In comparison to the maximum flame

speeds at periodically appearing, low blocking obstacles the maximum flame speeds are significantly higher with high blockage ratios for insensitive mixtures (s. fig. 2.8). If the flame front undergoes a transition to a detonation (fig. 2.8, 24 vol.% H_2), then the detonation velocity within an obstacle path of a high blockage ratio is lower than the detonation velocity within a low blocking obstacle path due to the corresponding pressure losses. The effect of flame acceleration by turbulent jets characteristically shows a significant dependence on the obstacle spacing. Of course there is a decreasing accelerating effect with an increasing obstacle spacing resulting in a decreasing coupling of the physical processes between the obstacles. On the other hand a very narrow obstacle spacing lets the flow behave like a flow in a smooth channel of a smaller diameter without jet formation, which again decreases the flame acceleration. Obviously there exists an optimum obstacle spacing, where the separated jet is able to reattach between the obstacles and a new accelerating jet is formed at the next obstacle (s. fig. 2.8).

3. CONCLUSIONS

The present paper gives a short introduction to the unstable dynamics of lean H_2-air flames, which is mainly caused by the interaction of pressure waves with the flame front and by preferential diffusion of the deficient reactant. Laser-optical visualization methods were used to phenomenologically demonstrate these effects.

The unstable dynamics of the flame front gets into interaction with the vorticity of the combustion induced expansion flow. The typical influence of the vortex-flame interaction has been discussed with respect to the typical length scales of the vorticity and the corresponding time scales in comparison with the chemical time scale. From that behavior an analytical burning law was derived expressing the turbulent burning velocity as a function of the laminar burning velocity, the turbulent fluctuating velocity, the integral length scale and mixture properties.

Showing examples of various explosion tube experiments different modes of turbulent flame acceleration have been demonstrated. As a major conclusion from the experiments with a single, low blocking obstacle it turned out that no enduring flame acceleration can be achieved by the interaction of flame fronts with those obstacles, unless significant local phenomena in the obstacle vicinity could be observed. However, an unstable feed back mechanism leads to a strong flame acceleration with multiple repeated, low blocking obstacles. As a main reason for the strong flame acceleration by a single, highly blocking obstacle the re-ignition of partially quenched zones, which are enriched with radicals was found. Accordingly stronger flame acceleration is achieved by multiple repeated, highly blocking obstacles, if the spacing between the obstacles reaches an optimum value.

4. NOMENCLATURE

δ_l	laminar flame thickness	c_p	isobaric heat capacity
ϕ	fuel equivalence ratio	D	mass diffusivity
γ_{H2}	H_2-concentration in vol.%	Da	Damköhler number
λ	heat conductivity	k	Kolmogorov micro scale of turbulence
λ_T	Taylor micro scale of turbulence	K	Karlovitz flame stretch factor
ν	kinematic viscosity	Ka	Karlowitz number
ρ	density	L	integral length scale of turbulence
τ_c	chemical reaction time	Le	Lewis number, $Le = a/D$
τ_k	Kolmogorov micro time scale of turbulence	Re_L	turbulent Reynolds number ref. to L
		s_l	laminar burning velocity
τ_L	integral time scale of turbulence	s_T	turbulent burning velocity

a	thermal diffusivity $a=\lambda/(\rho c_p)$	u'	rms fluctuation velocity
BR	blockage ratio, ratio between blocked area and unblocked area		

5. ACKNOWLEDGMENTS

It is gratefully acknowledged, that the work presented in this paper has been supported by the German Ministry of Education, Science, Research and Technology BMBF.

6. REFERENCES

1. **A. C. McIntosh**, Influence of Pressure Waves on the Initial Development of an Explosion Kernel, AIAA Journal, Vol. 33, No. 9, September (1995)
2. **G. I. Taylor,** The Instability of Liquid Surfaces when Accelerating in a Direction Perpendicular to Their Planes, Proc. Roy. Soc. (Ser. A) 201, 192 (1950)
3. **N. Ardey, F. Mayinger, B. Durst,** Influence of Transport Phenomena on the Structure of Lean Premixed Hydrogen Air Flames, 1995 ANS Winter Meeting, Thermal Hydraulics of Severe Accidents, San Francisco 1995, In: American Nuclear Society Transactions vol. 73, TANSAO 73 1-522, ISSN: 0003-018X, (1995)
4. **R. Borghi**, On the Structure of Turbulent Premixed Flames; Recent Advances in Aeronautical Science, Eds.: C.Bruno, C.Casci; Pergamon Press; (1984)
5. **N. Peters**, Laminar Flamelet Concepts in Turbulent Combustion, 21st. Symp. (Intl.) on Combustion, The Combustion Institute; Pittsburgh; (1986)
6. **F. Mayinger, R. Beauvais**, Influence of the Flow Structure on the Propagation of Hydrogen-Air-Flames, final report BMBF no. 1500 810, (1994)
7. **G. E. Andrews, D. Bradley, S. B. Lwakabamba**, Turbulence and Turbulent Flame Propagation - A Critical Appraisal, Comb. and Flame, Vol.24; (1975)
8. **G. Z. Damköhler**, Elektrochemie Angewandte Phys. Chem. 46, 601 (1940)
9. **D. B. Leason**, Fuel 30, 233 (1951)
10. **Brehm N., Mayinger F.**, Ein Beitrag zum Phänomen des Übergangs Deflagration - Detonation, VDI Forschungsheft vol. 653/1989, pp. 1-36, (1989)
11. **G. Strube**, Strucktur und Brenngeschwindigkeit turbulenter, vorgemischter Wasserstoff-Flammen, Dissertation TU München, (1993)
12. **R. Beauvais**, Brennverhalten vorgemischter, turbulenter Wasserstoff-Luft-Flammen in einem Explosionsrohr, Dissertation TU München, (1994)
13. **Brehm N., Mayinger F.,** Grenze für den Übergang von der Deflagration in die Detonation in Wasserstoff - Luft - Wasserdampf - Gemischen, Abschlußbericht BMFT RS 1500712, FIZ4; Karlsruhe; (1988).
14. **Thibault P., Yoshikawa N., Lee J. H.**, Shock Wave Amplification Through Coherent Energy Release, Fall Techn. Meeting of the Eastern Section of the Combustion Institute, Miamy Beach, (1978).
15. **H. Phylaktou, G. E. Andrews**, The Acceleration of Flame Propagation in a Tube by an Obstacle, Combustion and Flame, Vol. 85: pp 363-379, (1991)